Fall 2013

Insufficient CT data reconstruction based on directional total variation (DTV) regularized maximum likelihood expectation maximization (MLEM) method

Fahima Fahmida Islam

INSUFFICIENT CT DATA RECONSTRUCTION BASED ON DIRECTIONAL TOTAL

VARIATION (DTV) REGULARIZED MAXIMUM LIKELIHOOD EXPECTATION

MAXIMIZATION (MLEM) METHOD

by

FAHIMA FAHMIDA ISLAM

A THESIS

Presented to the Faculty of the Graduate School of the

MISSOURI UNIVERSITY OF SCIENCE AND TECHNOLOGY

In Partial Fulfillment of the Requirements for the Degree

MASTER OF SCIENCE IN NUCLEAR ENGINEERING

2013

Approved by

Hyoung Koo Lee, Advisor
Ayodeji Alajo
Xin Liu

ABSTRACT

Sparse tomography is an efficient technique which saves time as well as minimizes cost. However, due to few angular data it implies the image reconstruction problem as ill-posed. In the ill posed problem, even with exact data constraints, the inversion cannot be uniquely performed. Therefore, selection of suitable method to optimize the reconstruction problems plays an important role in sparse data CT. Use of regularization function is a well-known method to control the artifacts in limited angle data acquisition. In this work, we propose directional total variation regularized ordered subset (OS) type image reconstruction method for neutron limited data CT. Total variation (TV) regularization works as edge preserving regularization which not only preserves the sharp edge but also reduces many of the artifacts that are very common in limited data CT. However TV itself is not direction dependent. Therefore, TV is not very suitable for images with a dominant direction. The images with dominant direction it is important to know the total variation at certain direction. Hence, here a directional TV is used as prior term. TV regularization assumes the constraint of piecewise smoothness. As the original image is not piece wise constant image, sparsifying transform is used to convert the image in to sparse image or piecewise constant image. Along with this regularized function (D TV) the likelihood function which is adapted as objective function. To optimize this objective function a OS type algorithm is used. Generally there are two methods available to make OS method convergent. This work proposes OS type directional TV regularized likelihood reconstruction method which yields fast convergence as well as good quality image. Initial iteration starts with the filtered back projection (FBP) reconstructed image. The indication of convergence is determined by the convergence index between two successive reconstructed images. The quality of the image is assessed by showing the line profile of the reconstructed image. The proposed method is compared with the commonly used FBP, MLEM, and MLEM-TV algorithm. In order to verify the performance of the proposed algorithm a Shep-Logan head phantom is simulated as well as a real neutron CT image is tested to demonstrate the feasibility of the algorithm for the practical sparse CT reconstruction applications.

ACKNOWLEDGMENTS

TABLE OF CONTENTS

LIST OF ILLUSTRATIONS

LIST OF TABLES

NOMENCLATURE

Symbol	Description
FBP	Filtered Back Projection
MLEM	Maximum Likelihood Expectation Maximization
TV	Total Variation
MAP	Maximum-A-Posterior
DTV	Directional Total Variation
MAP-TV	Maximum A Posterior with Total Variation

1. INTRODUCTION

1.1. MOTIVATION

When irreplaceable and valuable objects are in the scope of an investigation, computed tomography (CT) is commonly used as the nondestructive evaluation technique to hold the integrity of an object. In this work for practical application neutron CT will be used. So the description of the CT will be discussed on the bases of neutron CT. X-ray CT is widely adapted for medical use to reconstructs the cross section image of a specimen. However, for some industrial use of CT such as for the nondestructive inspection of nuclear fuel, neutron computed tomography could be used as well. While X-rays and gamma rays which interact with the electrons of the atomic shell, and have the uniform attenuation increment with the atomic number are used for viewing heavy objects (high atomic number materials) in light materials (low atomic number materials), the neutron CT may be helpful to view light object wrapped in heavy materials, though the absorption or scattering of neutron does not show a linear dependence of the total cross section on the atomic mass. Therefore, as an evaluation technique, neutron CT can be used to great advantage for many cases.

Conventionally CT requires the 180 degree angular range of data for the cross sectional image reconstruction of the object. In many applications of computerized tomography, however, it is not possible or desirable to collect a complete set of data. For example, in cases such as electron microscopy, astronomy, geophysical exploration and non-destructive evaluation, data can only be collected over a limited angular range. The application of limited angle tomography constitutes a substantial advantage over conventional CT in that it can significantly reduce total imaging time, cost and radiation dosage applied to the image object or patient. Acquiring data for 180 degree angular range requires more time. So limited angle tomography is more desirable than conventional CT. However, limited angular view causes the lower quality image to interpret the evaluation. So the image reconstruction method is very important in limited angle tomography. It is desirable to design a reconstruction algorithm that takes into account different structure scales and yields a reduction in overall computational cost.

There are mainly two types of algorithm available for CT reconstruction. One is analytical method and another one is iterative method. The advantage of using iterative method over analytical method is the multiple repetitions of iterative algorithm in which the current solution converges towards a better solution. Although it is claimed that iterative algorithms takes more time than analytical method, using of some important regularization parameters make the iterative method faster as well as yield better image quality. Directional Total variation (DTV) regularization is one of the most important regularization parameter that is effectively used for limited angle CT to produce better quality image within reasonable computation cost.

1.2. ORIGINAL CONTRIBUTION

This thesis presents a novel algorithm that efficiently produces high-quality reconstructions for certain classes of neutron limited-data tomography reconstruction problems. As the emphasis is placed on the efficiency and effectiveness of the reconstruction algorithm, several other algorithms are presented to compare with and analyze the proposed method. Since much of the work reported within was motivated by the application to neutron computed tomography, the reconstruction algorithm used here are mostly applicable to neutron computed tomography though there are very little differences in principle of reconstruction algorithm for neutron CT and x-ray CT.

1.3. ORGANIZATION OF THESIS

This thesis is organized in the following way. Section 2 describes the theory and background of the thesis. This includes introduction to neutron , the basics of neutron imaging , the concept of tromographic imaging, history of and current trends in neutron CT ,basic apparatus used for neutron ct data acquisition, fundamental theory of image reconstruction, classification of limited angle CT, properties of limited angle CT, the short description of various reconstruction methods available for limited angle CT reconstruction. Section 3 describes the method of the proposed image reconstruction algorithm. Detail explanation of the method and mathematical background of applying the method are presented. Section 4 contains the result and analysis of the algorithm. Experimental analysis and quantitative evaluation is demonstrated in this section. The

evaluation criteria for image quality are briefly described in this section also. Section 5 presents the concluding remarks of this thesis.

2. BACKGROUND

This section presents some background of writing the proposed thesis. In this chapter, the introduction of neutron, neutron imaging, neutron CT, and the reconstruction method are described briefly.

2.1. INTRODUCTION TO NEUTRON

This section introduces the neutron with a short summary of its discovery and continues with a presentation of its properties like its interaction with matters and its cross sections.

2.1.1. Discovery of Neutron. The neutron was discovered as one of the constituents of the atom, well after its electrically charged companions the electron and the proton, for which there is some debate over any individual discoverer. In 1920, E. Rutherford proposed a close combination of electron and a proton as a neutral doublet, which he postulated would have novel properties of having the ability to move freely through matter. Therefore, it would be difficult to detect, and perhaps impossible to contain in a vessel. The term neutron was apparently first noted in the literature in a discussion on classifying isotopes in 1921 by W.D. Harkins. However, It took time to have the conclusive evidence for the existence of the neutron until 1932 when J. Chadwick reported first the possible existence and shortly thereafter the existence of the neutron. Chadwick received the 1935 Nobel Prize in Physics quite simply for the discovery of neutron [1].

2.1.2. Properties of Neutrons. Electrical neutrality is assumed to be the marked fundamental property of the neutron that makes it so useful in both neutron scattering and neutron imaging applications. According to Rutherford, as the neutron is uncharged, it interacts primarily with nuclei with highly penetrating characteristics and well able to investigate the interior of large assemblies; and as a significant additional benefit, it does so non-destructively.

Another basic property of the neutron is its mass, $m_n=1.6749XE-27$ Kg, which gives the neutron a de Broglie wavelength on the order of atomic distances for energies which is comparable to the excitations in condensed matter at room temperature [1]. Therefore, the neutron is simultaneously sensitive to both length and time scales relevant

to condensed matter. This is particularly relevant to neutron scattering applications; but the microscopic response to length scales is also important for imaging applications, particularly for polycrystalline materials in which the primary attenuation is due to Bragg scattering from the crystal lattice. The de Broglie wavelength, λ in units of nm, is given by

$$\lambda = \frac{h}{m_n v} = \frac{395.6}{v} \tag{1}$$

Where $h = 6.6261 \times 10^{-34}$ J× s is Planck's constant and v is the neutron velocity in ms^{-1}. The neutron energy, E in units of meV, is given by

$$E = \frac{1}{2} m_n v^2 = 5.2270 \times 10^{-6} \, v^2 \tag{2}$$

A neutron with an energy characteristic of 25.85 meV at a room temperature of 300 K, will have a velocity of 2224 ms^{-1} and a wavelength of 0.18 nm. The neutron carries momentum as expressed by its wave vector $\vec{k}$. The direction of $\vec{k}$ is that of the neutron, while its magnitude $|\vec{K}| = \frac{2\pi}{\lambda}$.

Other basic properties of the neutron include an associated nuclear magnetic moment of $-0.9662 \times 10^{-26} \, JT^{-1}$ and its intrinsic spin of ½. Thus in addition to nuclear interactions, the neutron will interact with the magnetic moments of unpaired electrons in matter. Neutrons are loosely assigned to band of energies associated with characteristic moderator temperatures, as shown in Table 2.1.

Table 2.1. Classification of neutrons [1]

Neutron Classification	Energy (meV)	Velocity (m/s)	λ (nm)
Ultra-cold	0.00025	6.9	57
Cold	1	437	0.9
Thermal	25	2187	0.18
Epithermal	1000	13832	0.029

2.1.3. Interaction with Matter and Cross Sections. In neutron imaging applications, the primary interest lies in neutron interactions that attenuate a well-defined incident beam of neutrons. Neutrons can be removed from the incident beam either by absorption or by a change in direction as they interact with material in the beam which is called scattering. More often, attenuation related to neutron absorption gives the clearer images than those related to neutron scattering. The absorption and scattering interaction are shown in Figure 2.1.
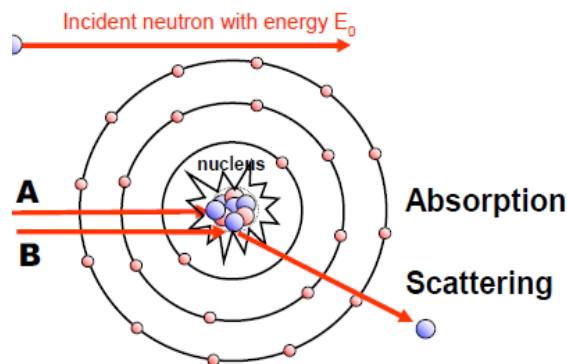
Figure 2.1. Absorption and scattering of neutrons [1]

The cross section quantifies the probability that a reaction will take place between the neutron (travelling at some effective velocity) and the target material; it can be considered as a target size and it is measured in cm^2. There are several types of cross section but the two that are of principal interest to neutron tomography are the absorption cross section and the scattering cross section. The total cross section is the some of these two. The unit of cross section is the 'barn', which is 10^{-24} cm^2, and typically cross sections vary from a few millibarns to several thousand barns. The cross section of the elements and their isotopes vary with the energy of the bombarding neutrons. In general, the lower the energy the higher the cross section. This fact provides the opportunity to increase the transmission of the neutron through the sample

2.2. THE BASICS OF NEUTRON IMAGING

As a fundamental particle, the neutron shows many unique attributes that is very useful for imaging techniques with a variety of contrast mechanisms. Neutron imaging has long been known to provide complementary, nondestructive imaging capabilities to

X-ray and gamma-ray imaging methods. The neutron imaging principle based on its cross-section properties. Any analysis of a neutron image, be it film or electronic, begins with an understanding of how the image is formed. The relationship between the incident neutron intensity upon an object to be imaged and the transmitted neutron intensity (ignoring scattering) is the simple exponential attenuation law:

$$I = I_0 e^{-\Sigma t} \tag{3}$$

The transmitted neutron intensity, I, is a function of the incident neutron intensity I_o and the product of the total macroscopic cross section and thickness of the object, Σt. Macroscopic cross section is the product of microscopic cross section (σ) and number density (n) of the matter.
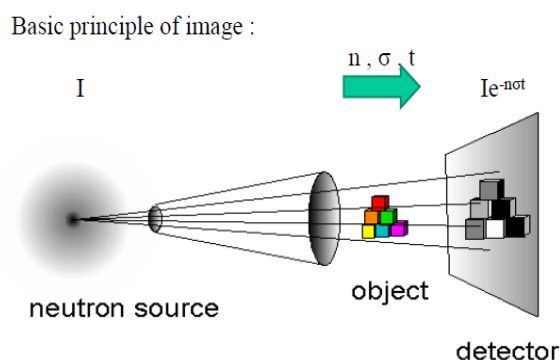
Figure 2.2. Principle of transmission image formation

The visibility of objects from neutron CT depends on the absorption cross section of neutron with that objects. The higher the absorption cross-section of neutron with the object is, the more visible the object will be. Since the principle of neutron attenuation is not based upon the same principle of x-ray attenuation, the objects that are poorly visible with x-ray imaging are easily visible with neutron imaging. For example a piece of paper in a glass container wrapped in a lead fuel can be better seen with neutron images than with x-ray images because smaller number of neutron than x-ray are attenuated by lead. Figure 2.3 shows the mass attenuation coefficient of x-ray and neutrons for different atoms.

After imaging whether it is film or digital imaging system, it is very important to relate the image view with the imaging system. In the case of film, the degree of film darkening (photographic density, D_e) is related to the neutron exposure by the film's characteristic response curve. D_e will have a logarithmic nature as described by [1]

$$D_e = G \times (logE) \tag{4}$$
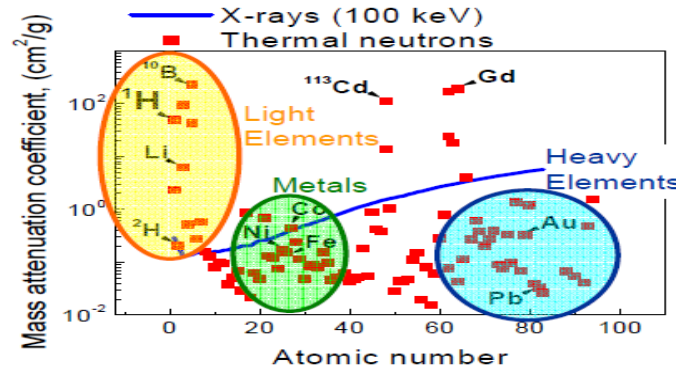
Figure 2.3. Attenuation coefficients of x-ray and neutrons in different elements

where E is the exposure of the film (transmitted neutron intensity multiplied by time, IT) and G is the slope in the linear portion of the characteristic response curve for the film being used; it is a parameter describing the manner in which a particular film responds to an exposure. This is the manner in which images are formed in film. One must bear in mind the when the images is being viewed, the processed film's photographic density is described by

$$D_e = \ln\left(\frac{\phi_o}{\phi}\right) \tag{5}$$

where ϕ_o is the incident light (such as from a light box) and ϕ is the transmitted light through film.

In nearly all forms of digital imaging, the resulting gray level value of any pixel making up the image may be described by

$$G = (C \times I) + G_{offset} \tag{6}$$

where G is the numerical gray level value of the pixel within an image, C is the electronic gain of the camera or imaging system (a constant), I is the transmitted neutron intensity and G_{offset} is the dark current, an additive offset due to electronic noise [1].

2.3. NEUTRON COMPUTED TOMOGRAPHY

In this section, the principle of computed tomography, the history and common trend of neutron CT, the apparatus used for neutron CT and the introduction of the techniques available for neutron CT are concisely described.

2.3.1. The Concept of Tomographic Imaging. Neutron computed tomography is a powerful tool for non-destructive testing of materials and finds numerous applications in industry and in material research as well. The basic principle is similar to that of X ray tomography. Tomography and radiography are well known from their uses in medicine and many people have already come into contact with one or more of these methods. They are closely related because tomography is based on radiography, which is a two dimensional attenuation coefficient distribution or the cross section of a ray-path-integrated projection from a three dimensional object. An extension of this two dimensional method (radiography) is tomography in which many projections of the same object is taken in different orientation and then the set of projections are used to reconstruct a three dimensional image. From different projections of one cross section, a two dimensional image can be formed. If these two dimensional images of different position are stacked together, the three dimensional view will be obtained. In other words, if line integrals (referred to as projections) of a property of a body are acquired such that these line integrals cover the area at all angles of a slice through the body, then the interior density of the slice can be reconstructed from these projections. The process of reconstruction is called tomography and the image of the interior spatial density is known as the tomographic image.

There are multiple steps involved in the whole reconstruction process. First a fixed number of beam of neutrons are directed from source through an object at a particular direction [1]. The number of neutrons from each beam passing through the object is recorded by neutron detectors, and this is called a projection view. Next, the object is rotated, and the projection process is repeated. Conversely, the object can be

held stationary, and the configuration of neutron source and detector can be rotated. The key concept behind this process is that each projection view occurs from a different direction or angle, and thus providing the additional information about the internal structure of the object. The set of projections are taken in different direction at a fixed rotational increment. Once the desired number of views is obtained, an image of the internal structure of the object can be computed from the projection view using various techniques.
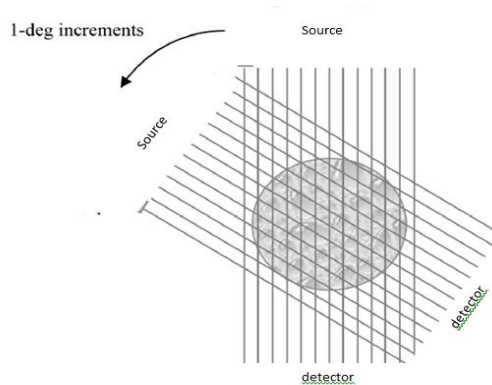
Figure 2.4. Method of acquiring projections[9]

2.3.2. History and Current Trends of Neutron CT. Neutron imaging has expanded rapidly as a means of Non-Destructive Testing of materials. Radiography with neutrons began shortly after the discovery of the neutron in 1932. The initial experiments in neutron radiography were performed in Germany in the late 1930's by H. Kallmann and E. Khun. In the years 1935 to 1938 H. Kallmann and Khun used Ra-Be sources and a small neutron generator at the research laboratory of the I.G. Farben Aktiengesellschaft to develop methods of photographic detection of neutrons. The next development of neutron radiography took place when nuclear reactor was invented for the first time in 1956 which produced the radiographs of much better quality than those of Kallmann and Khun. This technique developed slowly for several years until the advent of concept of computed tomography (CT) was discovered in 1960. Working with neutron CT expanded rapidly from that time to today.

Today, neutron CT with conventional reactor-based sources enables the interrogation of complex, multi-component systems for many applications, such as nuclear material nondestructive testing, characterizing flight control surfaces on aircraft, testing heat transfer in porous materials, examining heat exchanger systems, development of hydrogen fuel cells, inspection cultural heritage objects and interrogation biological systems. Newer, intense sources of neutrons from spallation facilities are providing the potential to interrogate time and energy dependent phenomena as well.

Nuclear application: Nuclear field is the place where neutron tomography applications started. Neuclear reactor use its neutron source to inspect the nuclear fuel and control material before and after irradation for comparison. To show the internal details and fission materials deposited in the central void of irradiated fuel, epithermal neutron tomography is very effective allowing good penetration. Other examples of nuclear neutron CT include determination burn-up in control materials, inspecting other nuclear components such as cold traps.

Archaeological and geological investigations: Archarlogical sector is the new application of neutron CT which was first reported in 1996. As most of the archaeological specimen are hydrogenous, neutron CT is very effective to give clear idea about them due to its characteristics of having high cross section with hydrogen. Besides, the high penetrating ability of thermal neutrons makes them a unique tool to investigate metal samples like historical weapons even when they are covered with thick calcareous concretions like in the case of finds from sunken ships. As an example, Neutron Tomography (Figure 2.5a) are shown for one sample of white calcitic marble recovered from the Villa Adriana (Tivoli, Italy) shown in Figure 2.5b.

Aerospace application: There is a huge application of neutron tomography in aerospace industry. The use of neutron tomography to detect corrosion in aircraft structure helps to redesign and operate the practical inspection facility for aircraft maintenance. Some major examples of neutron CT in aerospace sector are the inspection of assemblies to detect rubber or plastic seals, detection of adhesives in bonded assemblies and inspection of explosive devices.
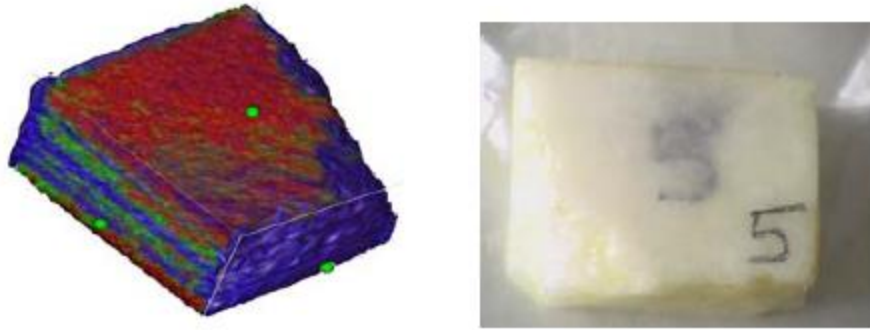
Figure 2.5. (a) Computed tomography of a (b) Calcitic marble [1]

Dynamic/Motion Application of neutron tomography: Neutron time laps tomography can be used to study the dynamic or motion behavior of any system by using dynamic detectors such as neutron image intensifiers and scintillator-camera systems. To obtain useful information from extensive rapid motion event, very fast image frame rates are required with high speed devises like high speed camera and pulsed reactor. For example, the general rates at which images are observed for dynamic events are as high as 10,000 frames/second. The neutron tomographic application for dynamic events can led to redesign of any motion system to work easily during system operation. The application of dynamic neutron tomography includes observing thermal expansion of nuclear fuel material, liquid metal in the casting process, fluid flow in metallic assemblies, lubricant and fuels in engine, aircraft corrosion, hydrogen location in titanium, filters and moisture/water migration [1].

2.3.3. Basic Apparatus for Neutron CT Data Acquisition. A neutron tomography systems consists of a neutron source, a moderator to thermalize the neutron, an aparature and a collimator to organize the neutrons into a beam, and a detector to visualize the image.

Source: Neutron tomography requires, off course, a source of neutrons. There are three general types of neutron sources: accelerator, radioisotope and nuclear reactor. Two types of sources can be used. One is high flux sources and another one is smaller or portable sources. Nuclear reactors are the example of high flux sources and radioisotope decay is the example of smaller sources. Accelerator based neutron sources can be the example of both type.

Accelerators: Accelerator-based neutron sources are ones that accelerate and direct a beam of charged particles such as protons, deuterons and alphas on to a target, which then results the emission of neutrons. There are a variety of combinations of incident particle and target material that can be used. High energy protons can create large number of spalled neutrons from bombardment of heavy nuclei.
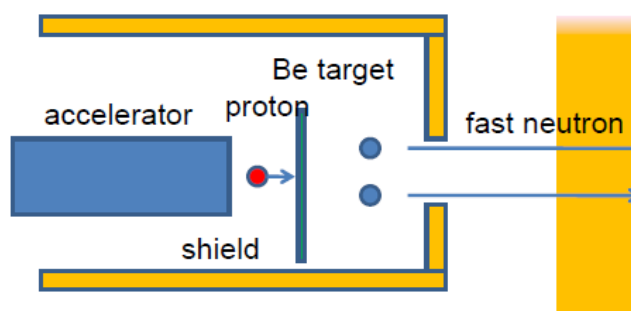
Figure 2.6 Principles of accelerators [12]

Table 2.2. Accelerator Neutron Sources [12]

Manufac-turer	Type	Particle	Target materials	Ope-rating voltage KV	Beam curre nt mA	Fast neutron output n/s	Neutron energy MeV
Elliot Automation 20th century	P Tube	Deuteron	Tritium	120	2	10^{11}	14
Electronics	NGH 150	Deuteron	Tritium	150	3.5	4×10^{11}	4
Sames	T	Deuteron	Tritium	400	3	10^{11}	2
High Voltage Eng. Co.	Van der Graaff	Deuteron	Berylliu m	3000	0.6	10^{10}	1.6
Mulfard	Linac	Electron	Berylliu m	5500	0.2	2×10^{11}	1.4

Small accelerator sources produce thermal neutrons in the range from 10^7 to 10^{10} n$\frac{cm^2}{s}$. Small accelerator sources produce thermal neutrons in the range from 10^7 to 10^{10} n$\frac{cm^2}{s}$ and offer the benefit of intermittent operation and portability. On the other hand, though large spallation sources can achieve fluxes of more than 10^{14} n$\frac{cm^2}{s}$, they are very complex and not portable.

Radioisotopic sources: There are no naturally occurring radioisotopes which emit neutrons. A radioisotope based neutron source allows the gamma rays or alpha particles emitted by the decay of a radioactive isotope to bombard a neutron emitting target. Table 2.3. shows a number of (Υ,n) and (α,n) radioisotopic neutron sources. Although these systems are simple in operation and ease of portability, they produce low thermal neutron fluxes in the range from 10^5 to 10^9 n$\frac{cm^2}{s}$. The other disadvantages it has are the inability to turn off the radiation and the decreasing number of neutrons because of the deterioration of the target and decay of the source [1].
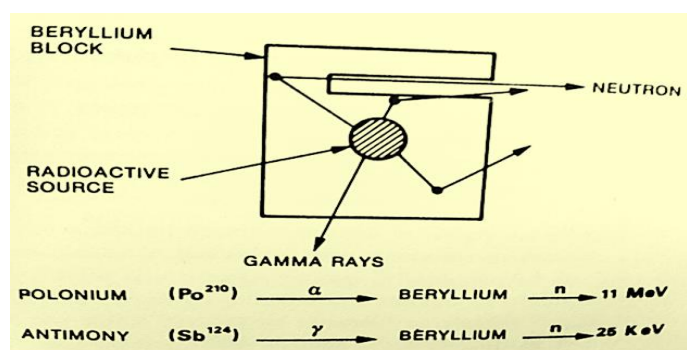
Figure 2.7. Isotopic neutron sources [12]

Nuclear reactors: Reactor based source produce neutrons from the fission reaction of uranium. For high quality neutron tomography, this source can be used as they provide intense neutron beams. These sources have thermal neutron fluxes within the range of 10^{10} to 10^{15} n$\frac{cm^2}{s}$ or even higher. However, large spallation neutron sources may provide neutron beams with intensities equal to or higher than those produced by nuclear reactors. Although the reactors

*Deuteron-Tritiated tubes:*These neutron sources are based upon deuteron beams impinging upon tritiated targets with relatively low accelerating potential and fairly high current with the resultant yield of 14 MeV fusion neutrons at a rate up to10^{11} n/s. These 14 MeV neutrons can be used directly for fast-neutron imaging as they are very penetrating in and of themselves.

Table 2.3. Radio isotopic Neutron Sources [12]

Source	Half-life	Reaction	Neutron yield $(n.s^{-1}g^{-1})$	Neutron energy (MeV)
^{124}Sb-Be	60 d	(Υ,n)	2.7×10^9	0.024
^{210}Po-Be	138 d	(α,n)	1.28×10^{10}	4.3
^{241}Am-Be	458 y	(α,n)	1×10^7	∼4
^{226}Ra-Be	1620 y	(α,n)	1.3×10^7	∼4
^{227}Ac-Be	218 y	(α,n)	1.1×10^9	∼4
^{228}Th-Be	191 y	(α,n)	1.7×10^{10}	∼4
^{252}Cf	265 y	fission	2.34×10^{12}	2.3

However, these high energy neutrons can also be used in epithermal, thermal or even cold neutron imaging by moderating them to a lower temperature. It has the advantage of portability that makes the infield application possible. With the small size of moderator it gives the higher contrast by yielding a small, bright source of neutrons.

Moderation: Neutrons produced in fission reaction or from spallation procedure possess very high energy peaking from 0.85 MeV from fission in reactor to 14 MeV in accelerators. However, for conventional neutron tomography the energy range of neutron should be in the thermal range of 0.025 eV to 10 KeV. For this purpose, the moderator is used.

Collimation: As neutrons have no charge, they cannot be focused directly to the object being imaged. They are scattered randomly in the moderator. In order to allow desired number of neutron beam to stream down toward the object being imaged, the collimator are used into or adjacent the moderator. A divergent collimator which spread

the lower neutron flax has small entrance aperture and larger exit. The wall of the collimator is lined with neutron absorbing material so that the stray neutron are prevented
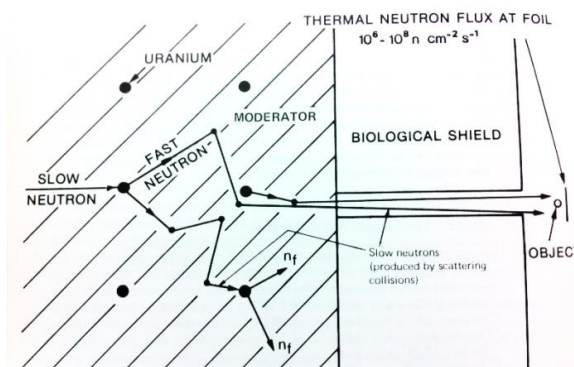
Figure 2.8. Thermal nuclear reactor Source [12]

to enter and the scattering of neutron become minimized. The angular spread depends on the L/D ratio which is a characteristic property of a collimator. The higher the ratio, the narrower the angular spread is [1].
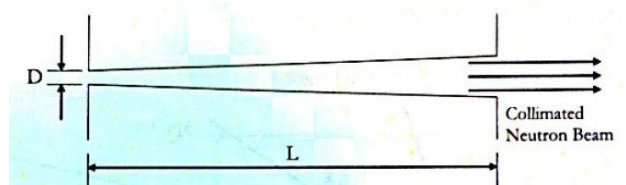
Figure 2.9. Neutron collimator [12]

Detector: Neutron has no charge so the only way to detect neutron is the detection of charged particles produced during the interaction of neutrons with matters. So, in tomography, the detector terms is applied collectively to both a converter and a recorder. The converter is used to emit alpha, beta or light which are more readily detectable radiation when encounter with neutron. And a recorder is used to record the emitted radiation. When film is used as image recorder gadolinium type foil is used and emits the electron during the exposure of neutron. the foil is placed with the direct contact with the recorder emulsion. When electronic form of imaging is used, a scintillator converter is coupled with an analog or digital camera image recorder. This allows the successive

record of the image that can be viewed directly on digital media with dynamic information. Different types of detector are used to detect the neutrons of different energies because the neutron interaction cross section in materials is dependent on neutron energies [1].
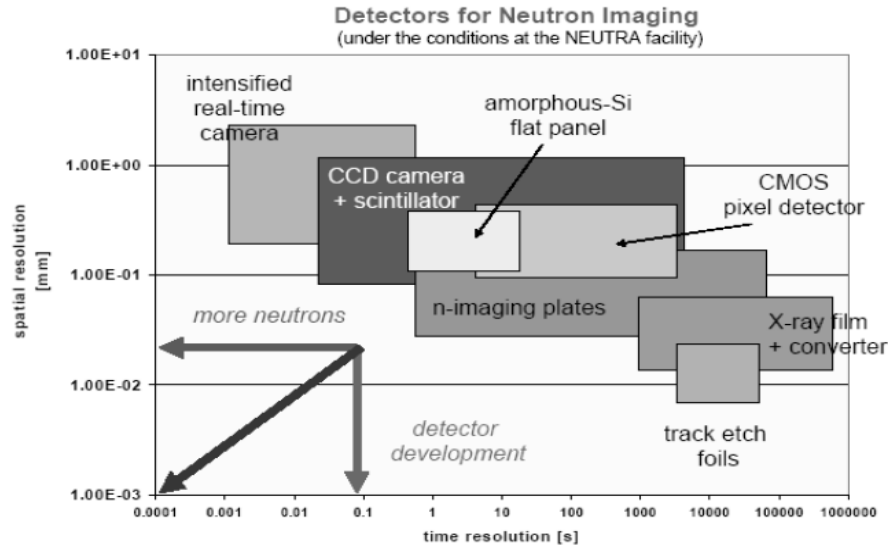
Figure 2.10. Performance of various detection systems [11]

2.3.4. The Radon Transform and Inverse Radon Transform. This section describes the fundamental physics of CT reconstruction with Radon transform. The projections of the object follow the radon transform to be obtained at different angles or views. So it is important to understand how radon transforms works. So in this section we will see the basis of radon transform [2] theory as well as the inverse radon transform which is used to obtain the back projection or the image of the object.

Since, Internal properties of objects are distinguished by differences in the attenuation coefficient of different materials, in neutron CT, the image of object is obtained by computing the amount of absorption of neutron by the object, or in other words, the attenuation of neutrons by the object or the cross section of neutrons for the object. So the projection will be the sum of the cross section over a specified distance or a specific beam line through the object. If a neutron beam of specific energy passes distance x through object for which the cross section is Σ the fractional decrease in intensity is given by,

$$\frac{I}{I_0} = e^{-\Sigma x} \tag{7}$$

Any two dimensional object is a function of two variables. These two variables are the spatial co-ordinate or the x and y coordinates in the rectangular (Cartesian) coordinate system. Let $\Sigma(x,y)$ designate the attenuation or cross section of neutron for the (x,y) position of the object. If L is the any beam of neutrons through the object, the fractional decrease in intensity is given by,

$$\frac{I}{I_0} = \exp[-\int_L \Sigma(x,y)ds] \tag{8}$$

where ds is an increment of length along L. The natural logarithm of above equation yield a sing projection,

$$P = -\log\left(\frac{I}{I_0}\right) = \int_L \Sigma(x,y)ds \tag{9}$$

In neutron CT, if there are some other parallel neutron beams coming from the source for the a fixed direction of ϕ, then the set of projections or profile for the angle ϕ would be,
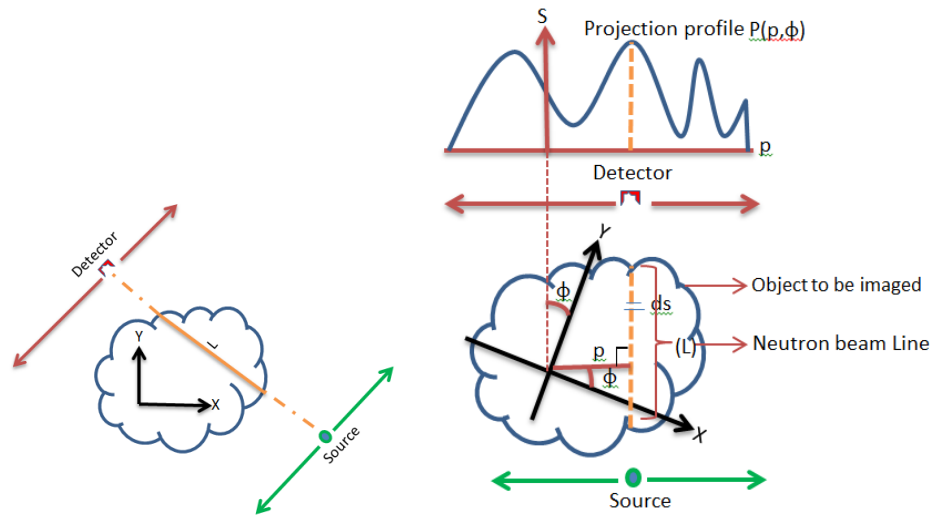
$$P(p,\phi) = \int_L \Sigma(x,y)ds \tag{10}$$

Figure 2.11. Radon transform

The mapping or projection or neutron beam line integral of *Σ(x,y)* along the beam line *L* through the object is the radon transform of *Σ(x,y)*. Explicitly,

$$P(p, \phi) = R\Sigma = \int_L \Sigma(x, y) ds \qquad (11)$$

R is used to define radon transform operator. One of the important property of radon transform is that *RΣ* can be uniquely determined from the integration along all lines *L* if and only if $\Sigma(x, y)$ is continuous and compact support.

So, *L* and *S* are the coordinate of the detector, the equation of neutron beam line *L* is

$$L = p = xCos\phi + ySin\phi \qquad (12)$$

and the equation of *S* would be

$$S = yCos\phi - xSin\phi \qquad (13)$$

Therefore, if we know *p* and ϕ, we can find out spatial coordinate of cross section and finding the *(x, y)* coordinate of *Σ* from p and ϕ is called the inverse radon transform or backprojection. *S* is a function of *p*, *S* is just the orthogonal value of *p*. So,

$$x = pCos\phi - sSin\phi \qquad (14)$$

$$y = pSin\phi + sCos\phi \qquad (15)$$

In one word, the radon transform or line integral is nothing but to convert the Cartesian coordinate in to polar coordinate system.

2.3.5. Neutron CT Reconstruction. CT reconstruction involves the reconstruction of a single slice. Stacking of such slices yields a 3D image. By means of image processing parts of the 3D reconstruction can then be extracted and displayed separately from the rest of the data set.

Neutron CT reconstruction is an inverse problem to solve. In neutron CT , the collection of the projection images from a physical body is the direct problem and the

corresponding inverse problem is the reconstruction of the unknown inner structure of the physical body from the known neutron projections taken from different directions [1]. There are several reconstruction methods applied to solve this inverse problem or neutron CT. For continuous tomographic data, analytical method or FBP is usually used which is based on inverse radon transform and for discrete data iterative reconstruction method is used. There are various model is used to discretize the object such as pixel based model, voxel based model, blob based model. In this thesis pixel based model is used [2]. Iterative method can be divided in to two categories based on the statistical model. If the statistical model is not considered, the iterative techniques include the large class of algebraic reconstruction techniques or ART methods which did not consider the noise in the data. In order to take account the effects of noise and background, statistical model based iterative reconstruction methods are used. The most common algorithm of statistical model based iterative reconstruction methods is MLEM (maximum likelihood expectation maximization). When the prior information of the image is known, Bayesian method is used to incorporate the prior knowledge of the image. The most common reconstruction algorithm which use the Bayesian technique is known as MAP or Maximum a Posterior algorithm.

2.4. LIMITED DATA NEUTRON TOMOGRAPHY

In this section, the classification of neutron data tomography and the nature of limited data CT are briefly described.

2.4.1. Classification of Limited Data Tomography. Limited data tomography is related to insufficient data to reconstruction [5]. There are many forms available for insufficient data. Some important forms are sparse sample which means the image reconstruction from projection data at few views, limited angular range and gaps in the projection data caused by bad detector bins.

In each of these three examples, the projection data are not sufficient for exact reconstruction or the unique solution of tomographic images For the case where the data are consistent but are not sufficient to determine a unique solution to the imaging model, the application of standard analytic algorithms such as filtered back-projection (FBP) will lead to conspicuous artifacts in reconstructed images.
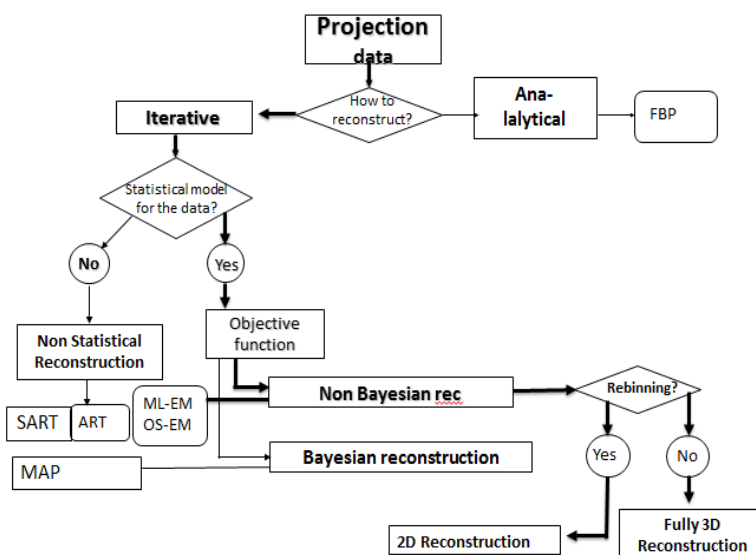
Figure 2.12 Methods of CT reconstruction
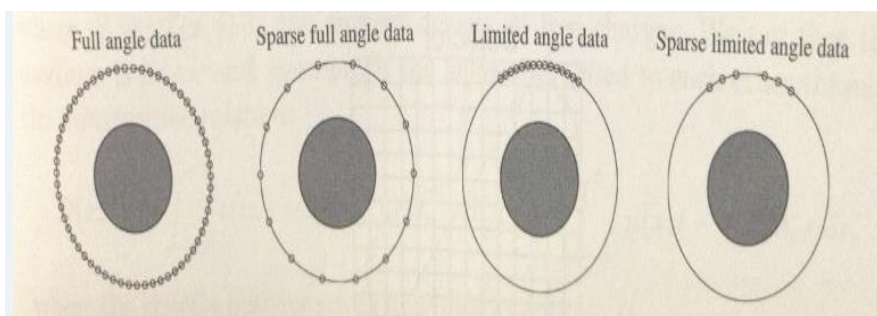
Figure 2.13. Different angular position of the detector [5]

2.4.2. Ill Posed Nature of Limited data CT. Image reconstruction is an inverse problem. For any inverse problem ill posedness is a characteristic [8]. Ill posedness is a characteristic that is defined by sensitivity of reconstruction to the measurement noise and modeling errors. Where there is not a unique solution of the reconstructed image and the solution is not dependent continuously on the true object then this type of nature is called the illposed nature of reconstruction.

In case of limited data projection, if the traditional analytical method is used to reconstruct the limited or insufficient data CT, the illposedness of the reconstructed image can be resulted in as the analytical method deals with the continuous

representation of the reconstruction problem. As this approach is established on the basis of the assumption that the projection data is available for all angles, in case of limited data CT problem this methods does not give the high quality reconstructed result. However, it is well established that the application of iterative method for the reconstruction of the limited data CT minimizes the illposedness of the reconstructed image as iterative method assumes the discrete representation of the problem and tries to minimize the error between the reconstructed image and the object iteratively.

3. MATERIALS AND METHODS

For limited angle tomography, a rigorous statistical reconstruction method that incorporated an accelerated regularized model was used. The convergence characteristics of this model were also included. The reconstruction process was carried out with MATLAB. In this section, each of the steps of the reconstruction process and the associated properties are described.

3.1. PHANTOM GENERATION

In order to validate the reconstruction algorithm, a 256×256 image is constructed according to the definition of the Shepp-Logan phantom. The Shepp-Logan phantom is the cross section of human head obtained using x-ray. There are 10 ellipses in Shepp-Logan phantom. The parameters of the ellipse are described below [10]:
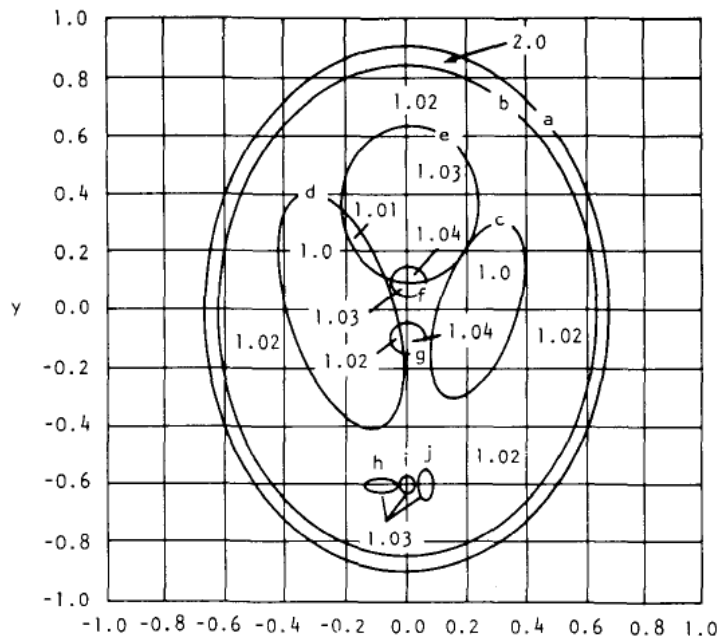
Figure 3.1. Construction of a Shepp-Logan phantom [10]

The refractive index of one ellipse indicates how less or more attenuating object the ellipse is than the surrounding ellipse or relative intensity.

3.2. SINOGRAM GENERATION

The sinogram for the Shepp-Logan phantom is created at 2.4^0 increments for 180˚.

Table 3.1. Properties of generating Shepp-Logan phantom [10]

Ellipse number	Center coordinate	Major axis	Minor axis	Rotation angle with respect to horizontal axis
A	(0,0)	0.92	0.69	90
B	(0, -0.0184)	0.874	0.6624	90
C	(0.22,0)	0.31	0.11	72
D	(-0.22,0)	0.41	0.16	108
E	(0,0.35)	0.25	0.21	90
F	(0, 0.1)	0.046	0.046	0
G	(0,-0.1)	0.046	0.046	0
H	(-0.08, -0.605)	0.046	0.023	0
I	(0, - 0.605)	0.023	0.023	0
J	(0.06, -0.605)	0.046	0.023	90

Figure 3.2. Process of generating sinogram

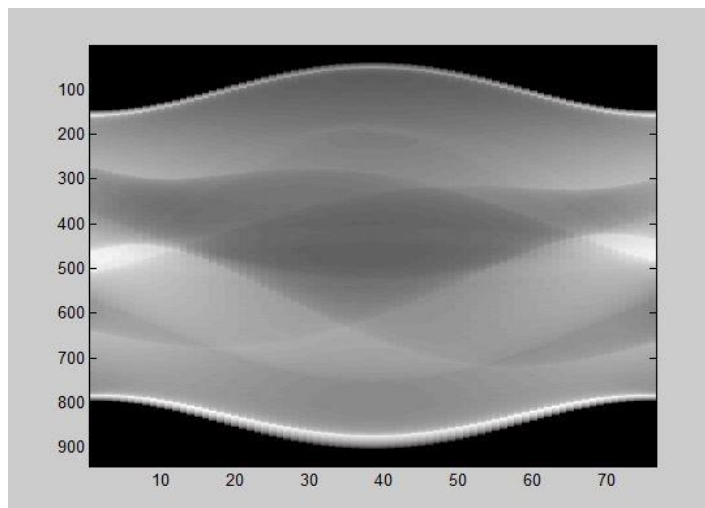### 3.3. NEUTRON IMAGE ACQUISITION

Neutron radiographs of the L07 fuel assembly are produced at the Neutron Radiography (NRAD) facility in Idaho National Laboratory (INL) using the near parallel beam geometry[7]. The assembly is rotated at 2.4˚ of precise increments with a radiographs produced in each increment. INL has developed an image acquisition system using transfer technique where x-ray films are used to image the irradiated nuclear fuel at NRAD. This technique involves a metal foil (Dy/ In) as the image recorder and captures the image by a buildup of radioactivity through neutron absorption. Thus an activation image is formed in the foil which is subsequently transferred in a photographic film by decay radiation. Metals like Dy/In emit beta particles sometime after neutron absorption, so, these metal foils are used as the detector and the radiographic image will be stored in the foil during the exposure. The screen is then removed from the neutron exposure and pressed against a suitable film in a cassette and the image will be formed to the film as the foil activity decays. The optical density (OD) measures the amount of decay in a certain point through an exposed and developed x-ray film. The OD is calculated through the attenuation formula, which assumes exponential beta decay inside the cassette [1].

3.4. SINOGRAM OF NEUTRON RADIOGRAPHS

Sinogram creation is the first step of the recostruction process from projections. The sinogram is created from the radiographs of different directions. The size of the radiographs should be the size of the detector. We have 76 radiographs of 941×941 size. For creating sinogram, we only consider one section of radiographs in different directions. One section of radiograph should be the one array of the detector. There are 941 bins in each detector array and 2.4˚ angular increment up to 180˚ angular range. So the total different angular directions are 76. If we place the projection of each bins in different directions we will get the sinogram.Therefore, the size of the sinogram should be 76×941.
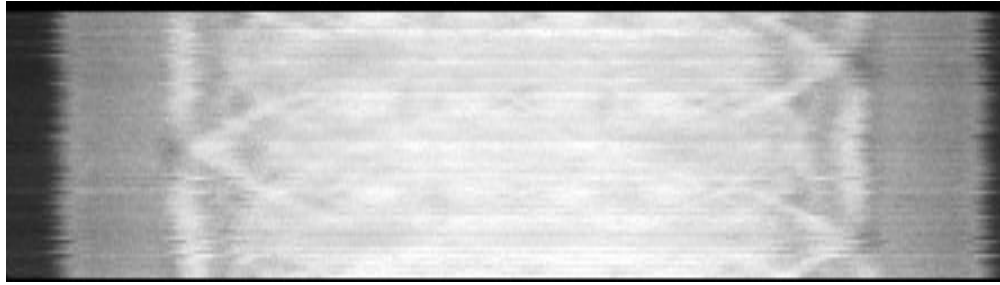
Figure 3.3. Sinogram of the fuel assembly.

3.5. IMAGE RECONSTRUCTION

An example is shown about how to calculate the projection and backprojection using radon transform.

Figure 3.4. Example of projection and back projection calculation.

The angle between the image y axis and detector p axis is ϕ, for $\phi=0$, and (x,y)=(0,0) position, the detector position will be,

$$p(xSin\phi + yCos\phi) = p(0) \tag{16}$$

and since, the pixel value of the position of (x,y)=(0,0) is v1;

$$p(0) = v1 \tag{17}$$

For the pixel position of (x,y)=(1,0) and ϕ=0, the detector position will be:

$$p(xSin\phi + yCos\phi) = p(1Sin0 + 0Cos0) = p(0) \tag{18}$$

As the pixel value for the pixel position of (x,y)=(1,0) is v7:
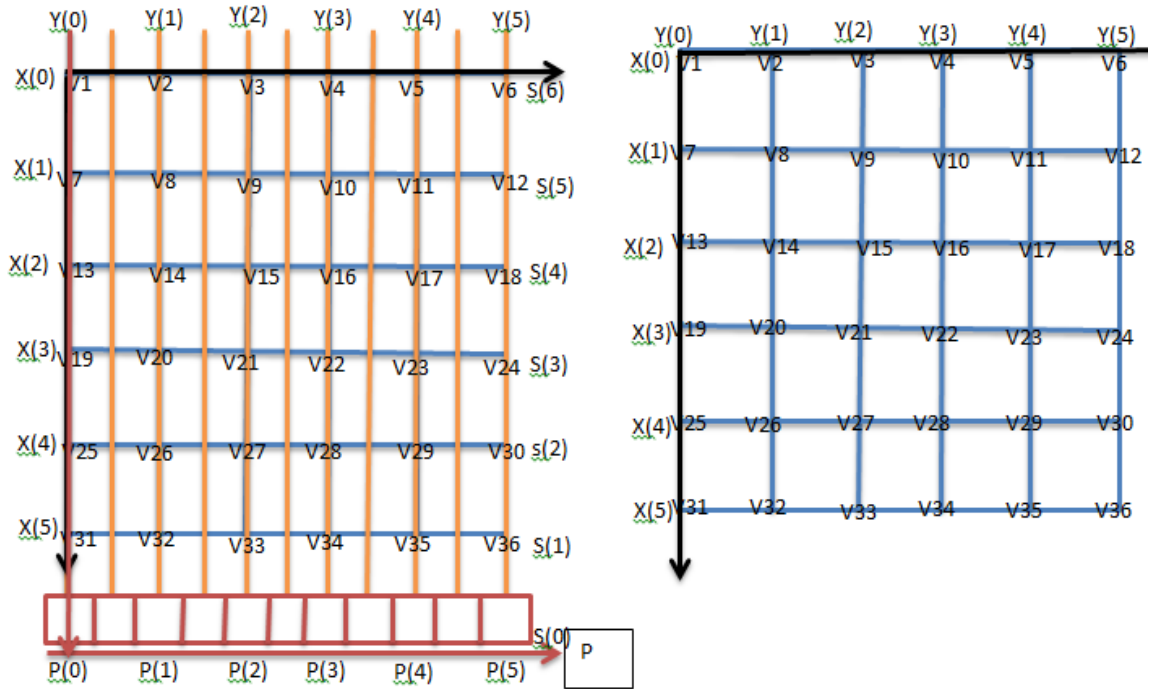
$$p(0) = v7 \tag{19}$$

Therefore, the final detector value for each detector position i for specific angle ϕ will be the summation of all the detector values for that position:

$$p(i, \phi) = \sum p(i) \tag{20}$$

$$p(0,0) = v1 + v7 + v13 + v19 + v25 + v31 \tag{21}$$

Similarly,

$$p(1,0) = v2 + v8 + v14 + v20 + v26 + v32 \tag{22}$$

Now, considering the angle between the image or pixel y axis and the detector axis is 45^0. Therefore, for ϕ=45^0, and (x,y)=(0,0) position, the detector position will be,

$$p(xCos\phi + ySin\phi) = (0Cos45 + 0Sin45) = p(0) \tag{23}$$

The intensity value for the (x,y)=(0,0) position is the v1,

$$p(0,45) = v1 \tag{24}$$

For the back projection:

$$s = p/tan\phi \tag{25}$$

$$x = pSin\phi + sCos\phi \tag{26}$$

$$y = pCos\phi - sSin\phi \tag{27}$$

To model the image system, the pixel number is kept half of the number which is one less than the bin number.

$$pixel\ number = \frac{1}{2}(bin\ number - 1) \tag{28}$$

The position axis of the image or pixel is chosen as the mid position of the pixel which is calculated as following [2]:

$$the\ position\ of\ x\ axis = \frac{number\ of\ row + 1}{2} \tag{29}$$

$$the\ position\ of\ y\ axis = \frac{number\ of\ column + 1}{2} \tag{30}$$

The proposed algorithm is made up of a model which incorporate the following assumptions that are specific for neutron CT measurements:

1. For neutron counting detector, the number of neutrons recorded by detector is a Poisson random variable.
2. In this case, since the neutron beam and the object are placed much closed to each other, the scattering effect is ignored.
3. The energy of source assumes to be mono-energetic (thermal energy).

3.5.1. Filtered Back Projection. Filtered back projection (FBP) is a well know technique for parallel beam image reconstruction. The algorithm involves the following steps:

1. Finding the 1D Fourier transform for each angle.
2. Multiply a filter with the result obtained from step 1.
3. Finding the inverse Fourier transform of the result obtained from step 2.
4. Back projecting the result obtained from step 3 to spatial domain.

The filter used in FBP is a high pass filter to reduce the blurring effect. The blurring effect is caused by the $|r|^{-1}$ no-uniform weighing, where

$$|r| = \sqrt{r_x^2 + r_y^2} \tag{31}$$

in the 2D Fourier plane. Applying various filters (e.g. Ram-Lak, Hamming, Han) reduces high frequency (i.e. noise) but enhances the blurring effect. Therefore, a perfect filter is difficult to construct without prior knowledge of the type of noise. A flow chart of the fbp algorithm is show in Figure 3.5 [9].
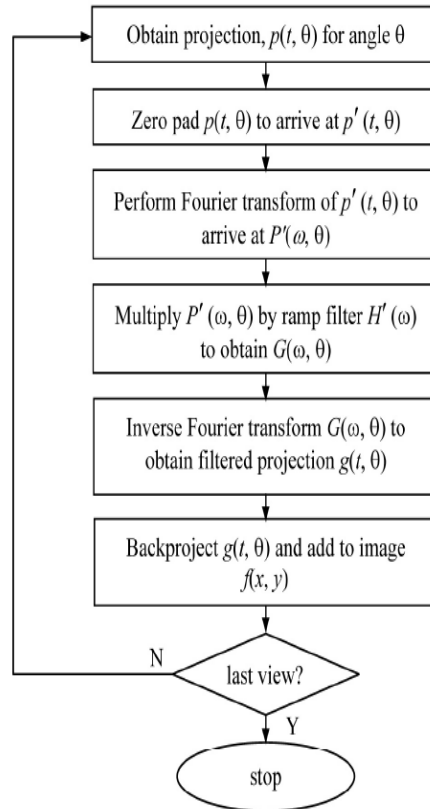
Figure 3.5. Flow chart of the FBP algorithm [9]

3.5.2. Iterative reconstruction. An iterative reconstruction algorithm developed as part of this work produces a better-quality image than the image obtained by conventional FBP. FBP algorithm utilizes integral equation but iterative algorithm uses algebraic equation which models complex imaging geometry and imaging physics more realistically. Another disadvantage of FBP is that it cannot model noise, and the noise control is achieved by frequency windowing.

3.5.2.1. Maximum- likelihood expectation maximization (ML-EM).

Maximum likelihood expectation maximization algorithm is used to reconstruct the L07 fuel bundle since it can model noise by minimizing an objective function. The ML-EM algorithm uses prior knowledge about the projection data to make the iterative algorithm more stable. Therefore, FBP reconstructed image is used as an initial guess. The general reconstruction algorithm for the ML-EM is [2]:

$$x_j^{new} = \frac{x_j^{current}}{\sum_{j=1}^{N} a_{ij}} \sum_{i=1}^{M} a_{ij} \frac{P_i}{\sum a_{ij} x_j} \tag{32}$$

P_i: measured projection

where P_i is the measured projection, x_j^{new} is the value of the pixel x_j after $(n+1)^{th}$ iteration, $x_j^{current}$ is the value of the pixel x_j after n^{th} iteration, Σa_{ij} is the weight of the contribution of pixel x_j to the projection P_i (backprojection of constant 1 in image domain), and $M \times N$ is the image size. The ML-EM algorithm has two steps:

E (expectation) step: estimation of observed data from current estimate of the model parameters and observed data

M (maximization) step: computation of the maximum-likelihood estimate of the model parameters using estimated observed data.

Convergence is an important criterion for any iterative algorithm. Each iteration of the EM algorithm includes a step to determine the likelihood of convergence. If the likelihood function converges, it returns to the E-step for next iteration.

ML-EM algorithm reconstructs images from limited data but the result is not useful enough. A regularization parameter is employed to obtain smooth image with sharp edge. Several methods (e.g. Bayesian and total variation) are used as a regularization parameter.

3.5.2.2. Total variation.
Total variation (TV) based [4] ML-EM algorithm is used to reconstruct L07 fuel bundle. Total variation measures how the signal changes between signal values, thus it measures the change in signal if any information is missing in between two rotation angles. In 1D, the total variation of N point signal is defined as:

$$TV(x) = \sum_{i=1}^{N-1} |x_{i+1} - x_i| \tag{33}$$

In 2D form, it can be written as:

$$TV(x,y) = \sum_{i,j=1}^{N-1}\left|x_{i+1,j} - x_{i,j}\right| + \left|x_{i,j+1} - x_{i,j}\right| \tag{34}$$

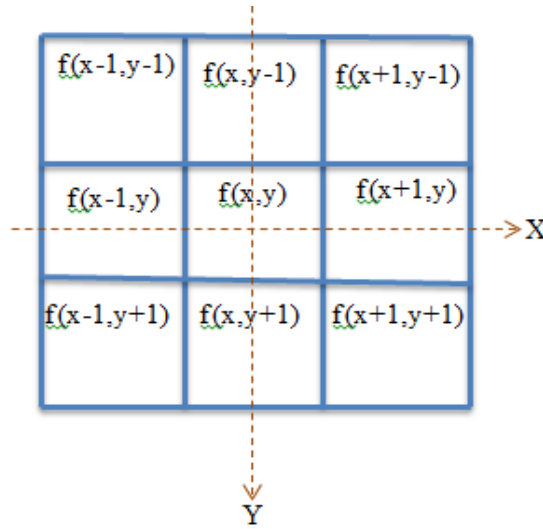| f(x-1,y-1) | f(x,y-1) | f(x+1,y-1) |
| f(x-1,y) | f(x,y) | f(x+1,y) |
| f(x-1,y+1) | f(x,y+1) | f(x+1,y+1) |

Figure 3.6. Position relationship between f(x,y) and its neighbor pixels

Implementing TV algorithm the TV regularized ML-EM algorithm can be written as [2]

$$x_j^{new} = \frac{x_j^{current}}{\sum_{j=1}^{N} a_{ij}+\beta\frac{\partial TV(X)}{\partial x_j}}\sum_{i=1}^{M} a_{ij}\frac{P_i}{\sum a_{ij}x_j} \tag{35}$$

where,

$$\frac{\partial TV(X_{i,j})}{\partial x_{k,l}} = \frac{x_{k,l}-x_{k-1,l}}{\sqrt{(x_{k,l}-x_{k-1,l})^2+(x_{k-1,l+1}-x_{k-1,l})^2+\varepsilon^2}} + \frac{x_{k,l}-x_{k,l-1}}{\sqrt{(x_{k+1,l-1}-x_{k,l-1})^2+(x_{k,l}-x_{k,l-1})^2+\varepsilon^2}} -$$

$$\frac{x_{k+1,l}+x_{k,l+1}-2x_{k,l}}{\sqrt{(x_{k+1,l}-x_{k,l})^2+(x_{k,l+1}-x_{k,l})^2+\varepsilon^2}} \tag{36}$$

where $x_{k,l}$ is a pixel of image x and ε is a penalized parameter [6]. The algorithm can be described in few steps as follows:

    3.5.2.3. Directional total variation. The previous total variation is independent in direction. To make the total variation of the image direction dependent, a weighing

function is used [3]. If the gradient of the image with respect to a particular pixel f(x,y) is $\nabla f_{x,y}$, the directional gradient along the α direction would be

$$\nabla_\alpha f_{x,y} = \omega(\alpha).\nabla f_{x,y} = \omega(\alpha).(D_x f_{x,y} + D_y f_{x,y}) \qquad (37)$$

where,

$$D_x f_{x,y} = f(x+1,y) - f(x,y) \qquad (38)$$

$$D_y f_{x,y} = f(x,y+1) - f(x,y) \qquad (39)$$

$\omega(\alpha)$ is the weighting function which only dependent on the direction of the image. It is uniform on the pixel values or the reconstructed image for parallel beam scan . So if we consider the directional total variation of the image

$$DTV = \omega(\alpha) \sum_{x,y} \sqrt{(D_x f_{x,y})^2 + (D_y f_{x,y})^2} \qquad (40)$$

$\omega(\alpha)$ calculates the summation of the contribution of all the views for a particular view of the image. So for the calculation of $\omega(\alpha)$, if the particular view of the image makes an angle of α with the x-axis, and the other views makes the angle of $\beta(\Theta)$ with the x-axis, where Θ is the angle between the detector and x-axis [3].
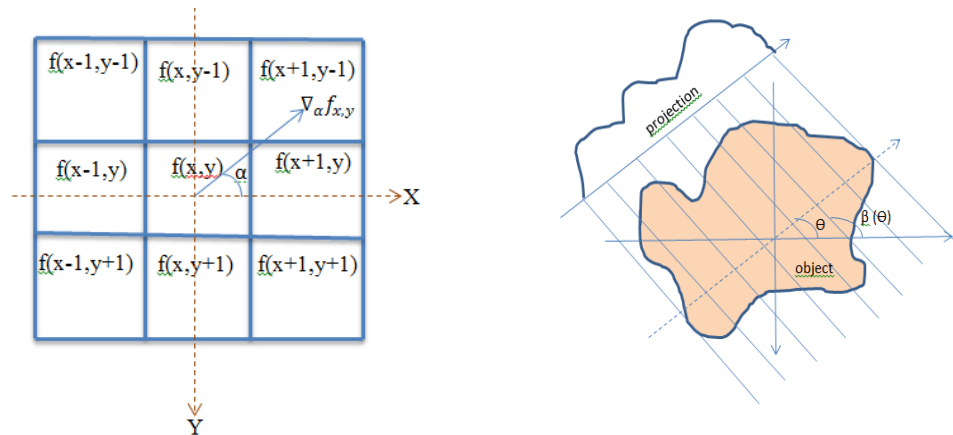

Figure 3.7. (a) Illustration of the calculation of the TV (b) projection geometry

$$\omega(\alpha) = \sum_\theta Cos(\frac{\pi}{2} - |\alpha - \beta(\theta)|) \qquad (41)$$

$$if \ \theta < 90^0, \qquad \beta = \theta + 90^0$$

$$if \theta > 90^0, \qquad \beta = \theta - 90^0$$

If there are more than one selected views,

$$\omega = \sum_\alpha \omega(\alpha) \tag{42}$$

3.5.2.4. Ordered subset expectation maximization. The convergence rate of MLEM is not so much high that's why it is necessary to increase the convergence rate. One way to speed up the convergence rate is to update the images more frequently. So, in that case order subset can be used. In case of order subset, the projection views are grouped in different sets. These sets are called subsets. The image is updated using each of the set in a specified order. The updating of the image using one subset is called the sub iteration. When all the subsets will be considered, then one iteration will be completed. There are many strategies available for grouping the views. It is established that increasing the number of subsets though increase the convergence rate, decrease the image quality [2].

3.6. PROPOSED TECHNIQUE

The proposed technique combines OS-MLEM with directional TV. The algorithm involves the following steps:

1. Initializing the image using FBP reconstructed image

2. Find out the projection of the FBP image

3. Compare the projection of the FBP image with the given projection (sinogram) by dividing given projection value by FBP projection for the projection views that are 9.47^0 apart from 0^0 to 180^0. Thus there are 4 subsets for 76 projections. Each subset has 19 projections.

4. Back projecting the compared projection (ratio) into the image for different angles.

5. Normalizing the image obtained from previous step by dividing this image by the image that is obtained from back projecting the value of '1' for different angles.

6. Updating the image reconstructed by MLEM by multiplying the normalized image with the initial image.

7. Applying the DTV minimization in the image obtained from previous step for different angles.

8. Adding the DTV minimized images with the updated image.

9. Ending the first sub iteration, for the next iteration, this updated image will be the initial image.

One iteration will be completed when all the subsets will be considered for iteration.

3.6.1. Algorithm of DTV-OS-MLEM. *Given:* The number of views (N_v), projections for different views ($p_i\ where, i = 1, \ldots.. N_v$).

Initialization and selection: Number of subset (*M*), Number of selected directional views(N_α), the weighting factor for selected direction($w_{i,}\ where, i = 1, 2 \ldots \ldots N_\alpha$), the number of iteration (N_{iter}), the mean difference between two intermediate image (ε_0). the initial image ($f^0 = FBP\ image$)

Main iteration Loop:

$for\ each\ iteration, k = 1, 2, 3, \ldots \ldots \ldots \ldots \ldots \ldots N_{iter}$

$f^k = f^{k-1}$

    Sub-iteration loop:

    $for\ each\ subset, m = 1, 2, 3, \ldots \ldots \ldots \ldots \ldots \ldots M$

    MLEM updating:

$$f^{k,m} = \frac{f^{k,m-1}}{\sum_{i\in m} BP_{i\in m}(1)} \sum_{i\in m} BP_{i\in m} \left(\frac{p_{i\in m}}{\sum_{i\in m} FP_{i\in m}(f^{k,m-1})}\right)$$

    DTV Minimization:

$$DTVM = \sum_{i=1}^{N_\alpha} w_i \left(\frac{\partial TV(f^{k,m})}{\partial f_{x,y}^{k,m}}\right)$$

    DTVM with OSMLEM:

$$f^{k,m} = f^{k,m} + DTVM$$

    end

    Image Updating:

    $f^k = f^{k,M}$

    Exit Criteria:

    $\varepsilon^k = \overline{f^k} - \overline{f^{k-1}}$

    $if\ \varepsilon^k < \varepsilon^0\ then$

    exit

end

BP_i is the backward projection for i^{th} view which follows the inverse radon transform and FP_i is the forward projection for i^{th} view which follows the radon transform.

4. RESULTS

In this section, the experimental studies are carried out in order to evaluate the performance of the proposed algorithm. Study includes the evaluation of the reconstruction quality. In this experiment our proposed algorithm is compared with FBP, MLEM, MLEM-TV. In order to verify the performance of the proposed algorithm a Shep-Logan head phantom is simulated as well as a real neutron CT image is tested to demonstrate the feasibility of the algorithm for the practical sparse CT reconstruction applications.

4.1. EVALUATION CRITERIA

There are two types of metrics are used in order to analyze quantitatively the development of the CT algorithms. The first type measures the performance of the numerical iteration. It includes the iteration index, convergence index and the measurement fidelity index. And the second type evaluates the image quality using the metrics of root mean square error (RMSE) and the ratio of the image TV.

Iteration index (k): iteration index measures the total number of the iteration that has been through. K indicates the long computational time when the algorithm will take a longer time for which k is larger [3].

Convergence index ($\delta_c{}^k$): This index measures the degree of convergence of the algorithm by calculating the difference of the images obtained from two subsequent iterations.

$$\delta_c^k = \frac{1}{N_{pixel}}|f^k - f^{k-1}| \tag{43}$$

where, N_{pixel} is the total number of pixels, and f^k is the reconstructed image from a particular iteration.

Measurement fidelity index (δ_p^k): this index compares the forward projections of the reconstructed image with the given projections by taking the ratio of them

$$\delta_p^k = \frac{p}{p_{fw}^k} \tag{44}$$

where p is the given projection and p_{fw}^k is the forward projection of the reconstructed image for k iterations.

RMSE: This measure can only be used when the density distribution of the phantom is prior known. However, in the practical case, the measure is not available. It compares the reconstructed image with the true image.

$$RMSE: \sqrt{\sum_{x,y} \frac{(f_{x,y} - f_{x,y}^*)^2}{N_{pixel}}} \tag{45}$$

where $f_{x,y}^*$ is the true image and $f_{x,y}$ is the reconstructed image.

TV ratio (δ_{TV}): The value of noise parameter or degree of smoothness (ε) can be verified by calculating the ratio of the total variation of the reconstructed image to the original phantom from the following equation:

$$\delta_{TV} = \frac{||f_{x,y}||_{TV}}{||f_{x,y}^*||_{TV}} \tag{46}$$

where $f_{x,y}$ is the reconstructed image and $f_{x,y}^*$ is the original phantom.

4.2. STUDY WITH SHEP-LOGAN HEAD PHANTOM

A parallel beam CT scan is simulated which contains 76 views covering 180^0 equally with 2.37^0 angular increment. Each view contains 941 detectors. A 941 by 941 sized image is reconstructed using different algorithms. In order to verify the algorithm a 941 by 941 sized Shep-Logan phantom is created. FBP, MLEM, MLEM-TV, MLEM-DTV, OS-MLEM-DTV are studied. In all the TV cases the optimal value of ε is chosen as 0.05. The total number of selected direction is set to six which are 30^0 apart from 0^0 to 180^0. So the set of selected direction is $\{30^0, 60^0, 90^0 120^0 150^0 180^0\}$. For OS-MLEM-DTV, four subsets are selected for 76 views. Each view is 9.47^0 apart. δ_c^k, δ_p^k are used to determine the stopping criteria . When the two matrices stops decreasing or begin to oscillate the iteration will be terminated.

Table 4.1. shows the numerical evaluation metrics for neutron CT studies. Figure 4.2. shows the reconstructed image of Shepp-Logan phantom using FBP, MLEM, MLEM-TV, MLEM-DTV and OS-MLEM-DTV. The line profile of the reconstructed

images obtained from each of the methods are drawn in Figure 4.3. The comparison of line profiles of head phantom for various algorithm is shown on Figure 4.4.

Table 4.1. Evaluation metrics of various reconstruction methods for head phantom

Reconstruction Methods	Number of Views	N_{iter} (Number of iterations)	δ_c ($\times 10^{-6}$)	δ_p ($\times 10^{-3}$)	δ_{TV}
FBP	_	0	_	10.08	_
MLEM	_	20	0.04	0.56	_
MLEM-DTV	6	15	0.06	0.10	0.001
OS-MLEM-DTV	6	9	0.07	0.40	0.007

4.3. STUDY WITH REAL NEUTRON CT DATA

A real neutron CT data of a nuclear fuel [7] is used to verify the application of our algorithm in the practical case. The neutron CT data A parallel beam CT scan which contains 76 views covering 180^0 equally with 2.37^0 angular increment. Each view contains 941 detectors. A 941 by 941 sized image is reconstructed using different algorithms. In order to verify the algorithm a 941 by 941 sized Shep-Logan phantom is created. FBP, MLEM, MLEM-TV, MLEM-DTV, OS-MLEM-DTV are studied. In all the TV cases the optimal value of ε is chosen as 0.05. The total number of selected direction is set to six which are 30^0 apart from 0^0 to 180^0. So the set of selected direction is $\{30^0, 60^0, 90^0 120^0 150^0 180^0\}$. For OS-MLEM-DTV, four subsets are selected for 76 views. Each views are 9.47^0 apart. δ_c^k, δ_p^k are used to determine the stopping criteria . when the two matrices stops decreasing or begins to oscillate the iteration will be terminated. Table 4.2 shows the numerical evaluation metrices for nuclear fuel studies. Figure 4.4 shows the cross section of L07 fuel bundle. Figure 4.5 shows the reconstructed image of nuclear fuel using FBP, MLEM, MLEM-TV, MLEM-DTV and OS-MLEM-DTV. The line profiles of the reconstructed images obtained from each of the methods are drawn in Figure 4.6.

Original Shepp- Logan Phantom   FBP Reconstructed

MLEM Reconstructed   MLEM-TV Reconstructed

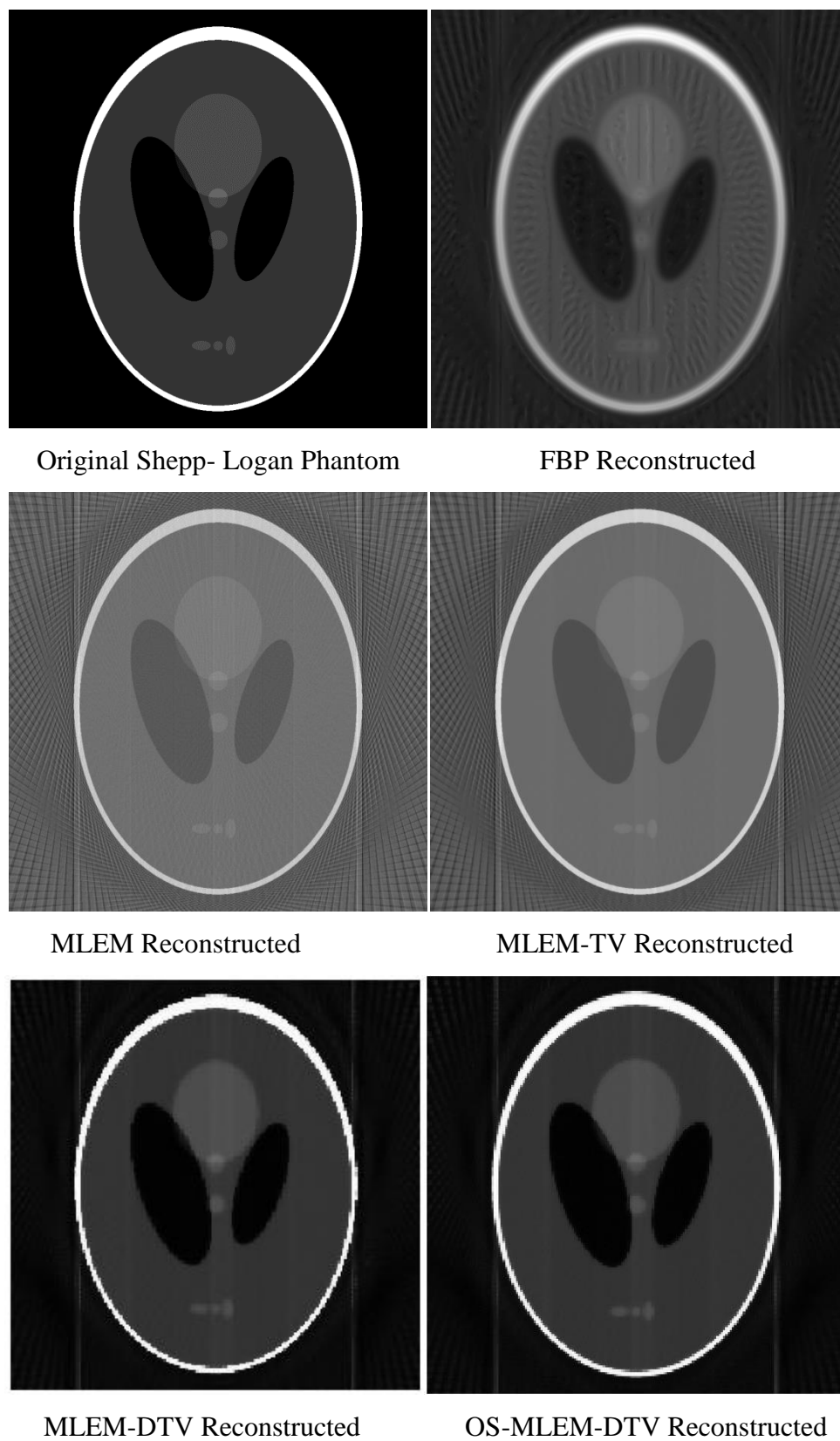MLEM-DTV Reconstructed   OS-MLEM-DTV Reconstructed

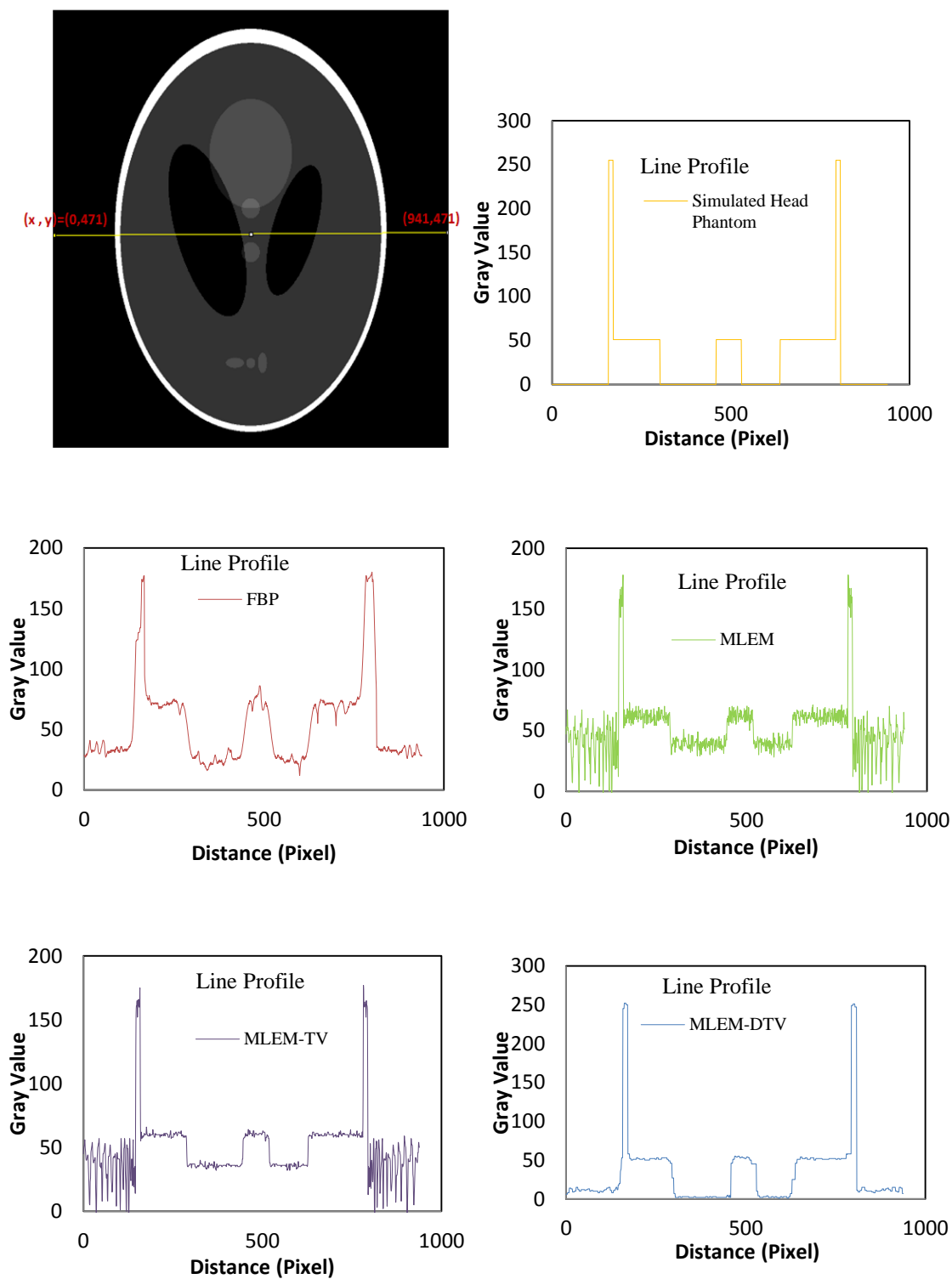Figure 4.1. Reconstructed image using various algorithms for head phantom

Figure 4.2. Line profiles for various reconstruction methods of head phantom
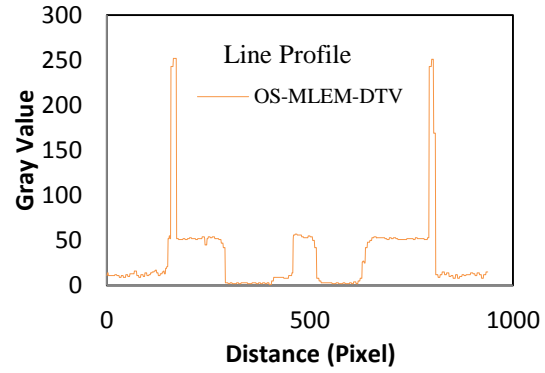
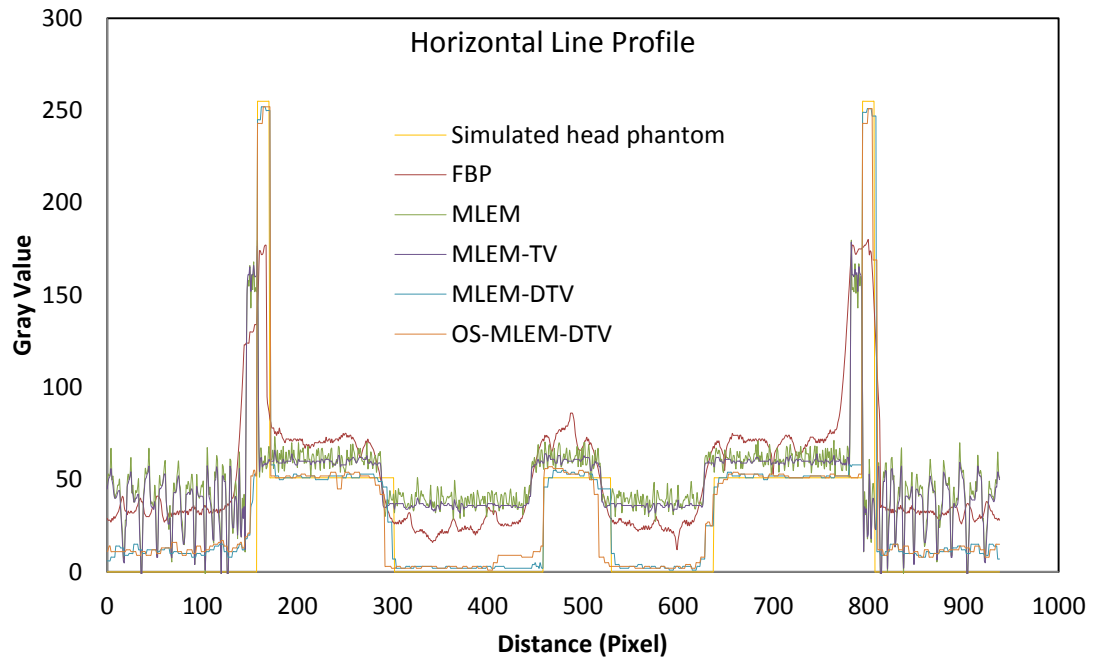Figure 4.3. Line profiles for various reconstruction methods of head phantom

Figure 4.4. Comparison of line profiles of head phantom for various reconstruction
algorithms

Table 4.2. Evaluation metrics of various reconstruction methods for nuclear fuel

Reconstruction Methods	Number of Views	Number of subsets	N_{iter} (Number of iterations)	δ_c ($\times 10^{-6}$)	δ_p ($\times 10^{-3}$)
FBP	–	–	–	–	15
MLEM	–	–	20	0.04	10
MLEM-DTV	6	–	15	0.002	4
OS-MLEM-DTV	6	4	10	0.0043	7
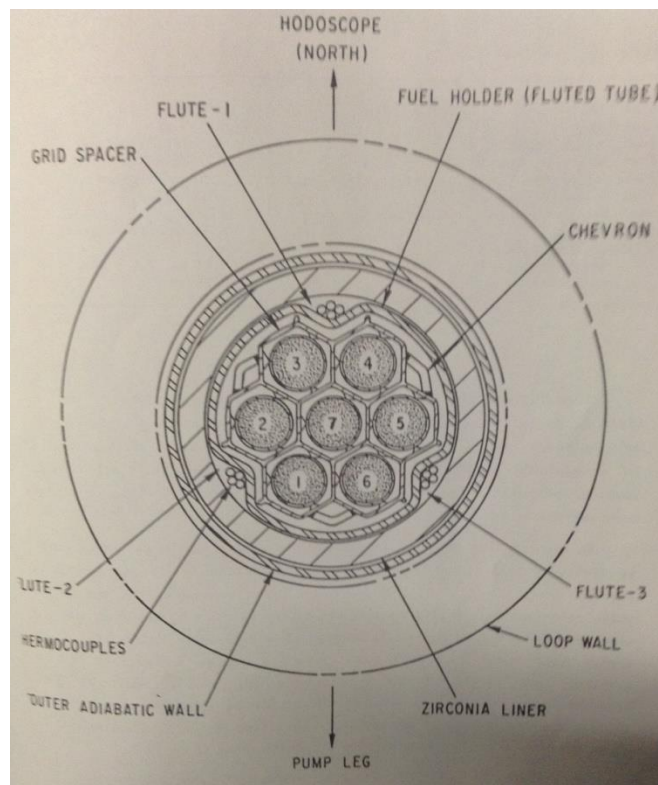
Figure 4.5 The cross section of L07 fuel bundle
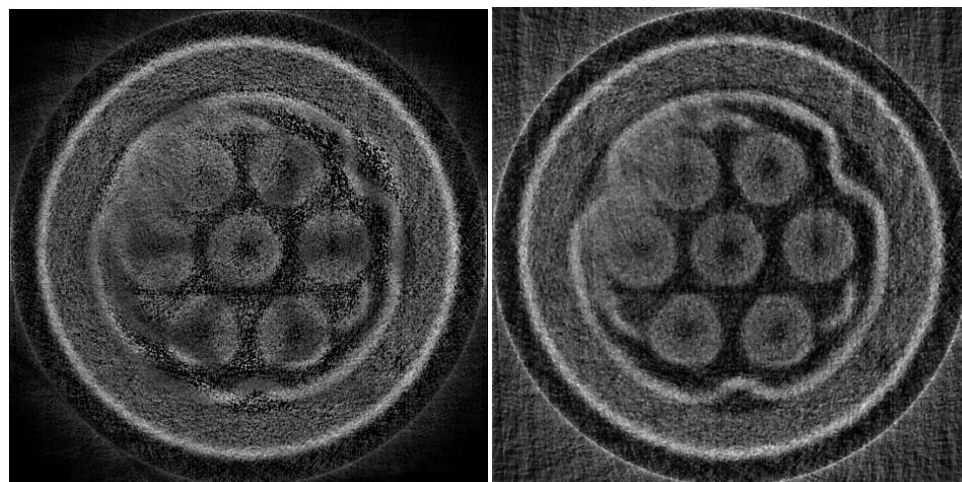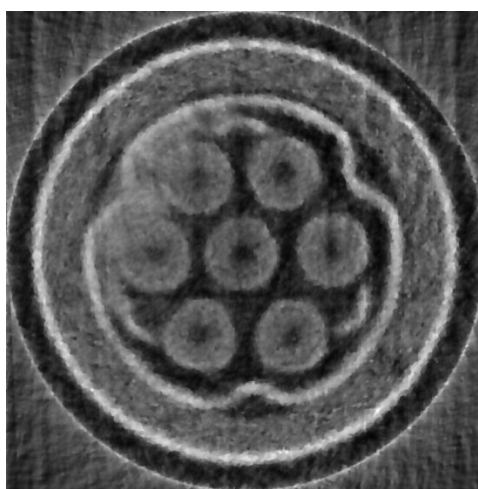
FBP Reconstructed   MLEM Reconstructed
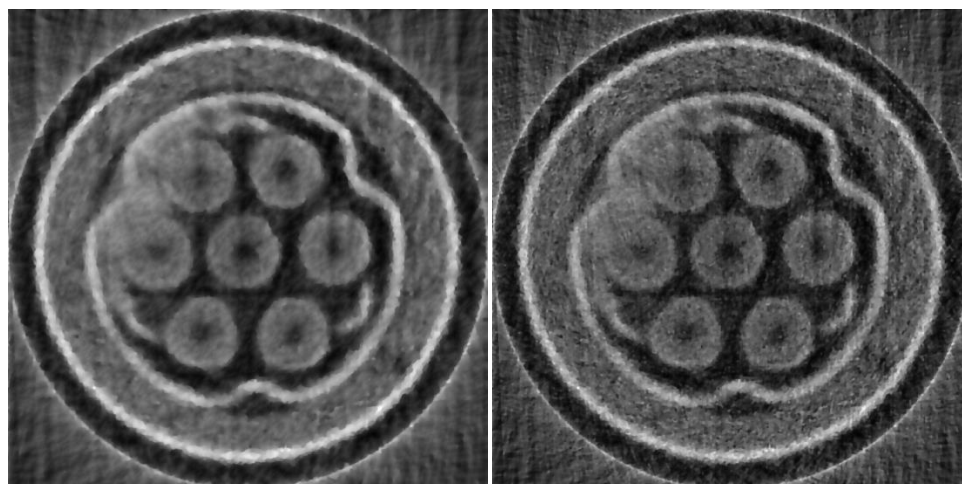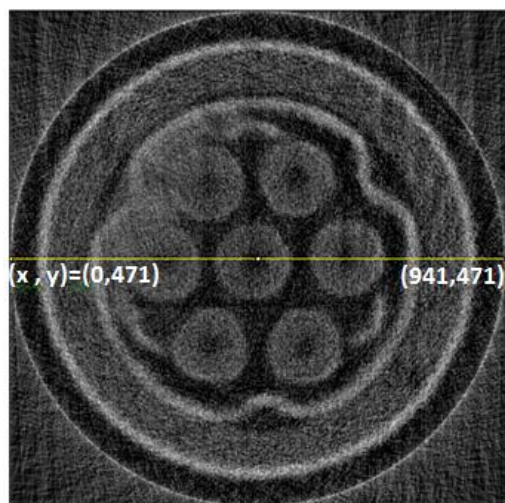
MLEM-TV Reconstructed   MLEM-DTV Reconstructed

OS-MLEM-DTV Reconstructed

Figure 4.6. Reconstructed image of nuclear fuel using various algorithm methods.
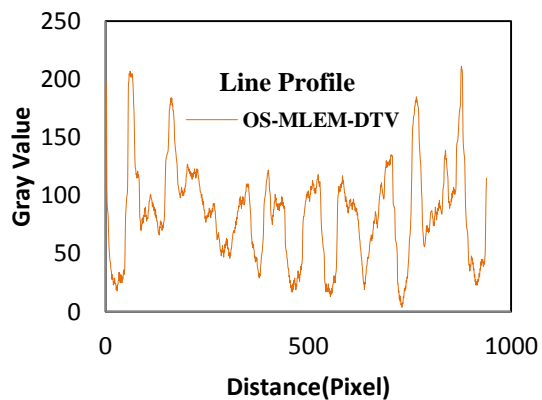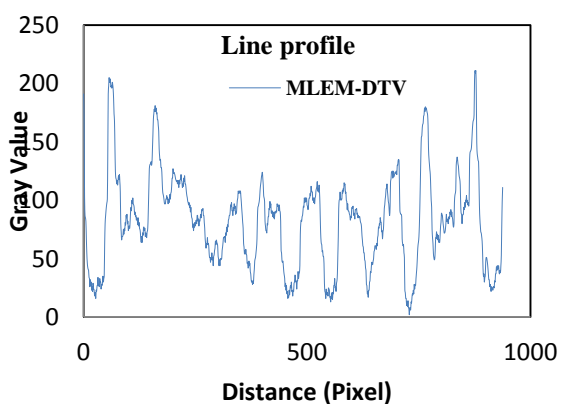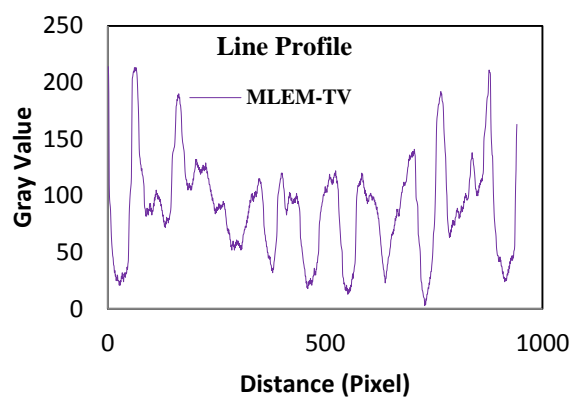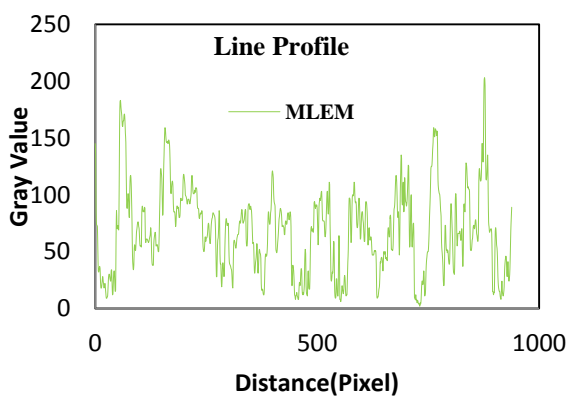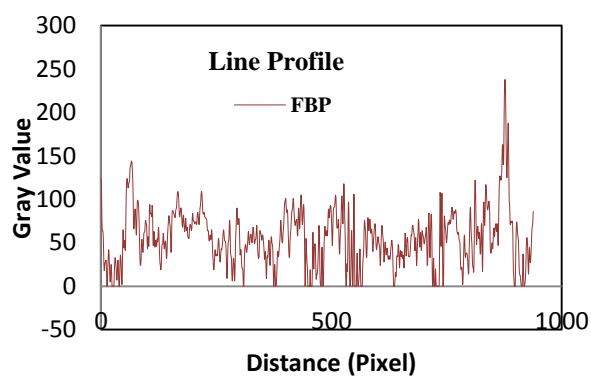
Line along which the profile drawn

Figure 4.7. Line profiles for various reconstruction methods of nuclear fuel

5. DISCUSSION AND CONCLUSION

It is shown from the line profile of the FBP reconstructed image that very little details can be observed with high oscillations. The MLEM reconstructed image line profile has very high oscillations. MLEM-TV gives the smoother image than MLEM but still far away from the truth profile. However, the smoothness is achieved because the MLEM only focuses on making an agreement between the measured data and the forwarded projection, while the TV added part focus on both the measurement agreement and smoothness property. Comparison of the reconstruction results with various algorithms for Shepp-Logan Phantom has shown that the MLEM-DTV method recovers more details and smooth out more noise than other algorithms. The profiles of the MLEM-DTV and OS-MLEM-DTV results are closest to the truth. It also shows that the image quality of MLEM-DTV and OS-MLEM-DTV is almost same. The use of order subset for MLEM-DTV is mainly due to increase the convergence rate.

While the study of Shepp-Logan head phantom shows the performance of the proposed algorithm, the test on real neutron CT data evaluates its potential in practical applications. In this case it is difficult to compare as there is no truth phantom available. However it can be shown that the MLEM-DTV and OS-MLEM-DTV maintains a better balance between the smoothness and the image details than the other algorithms.

In conclusion, it can be said that in sparse CT reconstruction, MLEM –DTV is very useful for getting almost exact reconstruction over other used methods. This method uses the directional total variation as a prior of the image and reconstructs the image by using MAP rule. The advantage lies in this method is that, it recover the better quality image which gives the better balance between the image details and the smooth property than that of other well-known methods.

BIBLIOGRAPHY

[1]   Ian S. Anderson, Robert L. McGreevy, Hassina Z. Bilheux, "Neutron Imaging Applications: A reference for the imaging community," Springer, 2009.

[2]   Zeng L. GengSheng, "Medical Image Reconstruction: A conceptual tutorial," Springer, 2010.

[3]   Chen Zhiqiang, Jin Xin, *et al,* "A limited-angle CT reconstruction method based on anisotropic TV minimization," *Physics in Medicine and Biology,* 2013, Vol. 58, 2119-2141.

[4]   Sidky Y. Emil, Kao Chien-Min, *et al,* "Accurate image reconstruction from few-views and limited-angle data in divergent-beam CT," *J. X-ray Sci. Tech.*, 2006, Vol. 14, 119-139.

[5]   Kaipio Jari, Somersalo Erkki, "Statistical and Computational Inverse Problems," Springer, 2006.

[6]   Das Mini, Gifford C. Howard, *et al,* "Penalized maximum likelihood reconstruction for improved micro calcification detection in breast tomosynthesis," *IEEE Trans. Med. Imaging,* 2011, Vol. 30(4), 904-914.

[7]   Morman J. A., Froehle P. H., "Tomographic Reconstruction of Fuel Assembly Configurations: PFR/TREAT Test L07 Lower Blockage Region," *ANL Technical Report,* 1989.

[8]   Muller L. Jennifer, Siltanen Samuli, "Linear and Nonlinear Inverse Problems with Practical Applications," Society for Industrial and Applied Mathematics, 2012.

[9]   Jiang Hsieh, "Computed Tomography Principles, Design, Artifacts, and Recent Advances," Wiley, 2009.

[10]   Avinash C. Kak, Malcolm Slaney, "Principles of Computerized Tomographic Imaging," SIAM, 1988.

[11]   Glenn F. Knoll, "Radiation Detection and Measurement," Wiley, 2010.

[12]   Heinz Röttger, "Neutron Radiography Handbook: Nuclear Science and Technology," Springer, 1981.

VITA

Fahima Fahmida Islam was born on October, 1987, in Dhaka, Bangladesh. She received her Bachelor of Science in Civil Engineering from Bangladesh University of Engineering and Technology, Dhaka, Bangladesh in October 2010. After graduation, being a part of researcher, she joined to Missouri University of Science and Technology (Missouri S&T) for pursuing her M.S. in Nuclear Engineering. She is planning to pursue her PhD after finishing her M.S.

Fahima held a Graduate Research Assistantship under Dr. Hyoung Koo Lee with the department of Nuclear Engineering at Missouri S&T. She will receive her Master of Science in Nuclear Engineering from Missouri University of Science and Technology in December 2013.